Systems & Control Transactions

Research Article - Peer Reviewed Conference Proceeding
ESCAPE 35 - European Symposium on Computer Aided Process Engineering
Ghent, Belgium. 6-9 July 2025
Jan F.M. Van Impe, Grégoire Léonard, Satyajeet S. Bhonsale,
Monika E. Polańska, Filip Logist (Eds.)

PSE PRESS

Design of Microfluidic Mixers using Bayesian Shape Optimization

Rui Fonseca* and Fernando Bernardo

CERES, University of Coimbra, Department of Chemical Engineering, Coimbra, Portugal
* Corresponding Author: ruifo@sapo.pt.

ABSTRACT

Microfluidic mixing has gained popularity in the Pharmaceutical Industry due to its application in the field of Nano-based Drug Delivery Systems (DDS). The flow conditions in Microfluidic mixers enable very efficient mixing conditions, which are crucial for the production of Nanoparticles by Flash Nanoprecipitation (FNP), as it enables reproducible production of particles with low-size variability. Mixer geometry is one of the most determinant factors, as it largely determines the flow patterns and the degree of contact between the two mixing streams. In this paper, a shape optimization methodology using Computational Fluid Dynamics (CFD) and Bayesian optimization is applied to the toroidal micromixer design, considering three different operating conditions. It consists of first defining a geometry solution space and then using Multi-Objective Bayesian optimization to explore the different designs. Mixer performance is evaluated with CFD simulations and two objective functions are considered: mixing time and pressure drop. Approximations of the Pareto front for each case study are obtained and the analysis of the best geometries enabled to derive some general geometric features of optimal mixer designs.

Keywords: Micromixing, Geometry Optimization, Multi-objective Optimization, Computational Fluid Dynamics.

INTRODUCTION

Mixing and mass transfer are fundamental aspects of many chemical and biological processes. Microfluidic mixing has recently gained much traction as an advantageous technology in the field of Nano-based Drug Delivery Systems in the Pharmaceutical Industry [1]. Several Drug products, such as peptides and nucleic acids, must rely on specialized nanostructures to protect the Active Drug Ingredient (API), and are therefore able to achieve the desired Drug Pharmacokinetic and Pharmacodynamic properties [2]. These systems, usually Nanoparticles, are synthesized by Flash Nanoprecipitation (FNP), which consists in the rapid dilution of a solution containing amphipatic molecules with an anti-solvent. This sudden change of solubility results in the rearrangement of the solute molecules and consequent formation of Nanoparticles [3].

The reduced channel size of Microfluidic mixers entails a high mass-transfer area/ volume ratio, which enables the very fast mixing of the two solutions. This reduces the mass transfer resistance during the FNP process, allowing the formation of particles of controlled size and low polydispersity, both critical quality attributes (CQA) of these products. Consequently, Microfluidic mixing is generally a more fit process to reproducibly comply with the tight quality demands of the product, when compared with the traditional alternatives [4].

Conceptually, Microfluidic mixing is merely the passive mixing of two solutions. Process optimization is therefore limited to the tuning of two operating parameters (Total Flow Rate (TFR) and Flow Rate Ratio (FRR) of the two inlet streams) and of the mixer's geometry. Optimizing the flow rates for a given geometry can be done experimentally with general Quality by Design (QbD) procedures. In contrast, mixer geometry optimization presents some challenges. The limitless degrees of freedom in mixer design ensue a very large number of experiments to realistically cover the broad solution space. Furthermore, the experimental evaluation of each design is in itself a cumbersome and expensive task, as it would involve the iterative design, fabrication and testing of each device.

In this paper, we present a systematic approach for

the geometry optimization of the toroidal micromixer. The adopted methodology begins with the comprehensive parametrization of the mixer geometry solution space, using continuous and discrete geometric parameters with established bounds. Mixer performance evaluation is achieved through the simulation of the Villermaux-Dushman reaction system [5-6] inside the mixer, using Computational Fluid Dynamics (CFD). Two metrics, pressure drop and mixing time, are then considered in the multi-objective optimization problem. The solution space is subsequently navigated employing a Bayesian optimization framework, by iteratively selecting the solution point most likely to improve the Hypervolume indicator. Three case-studies are presented considering different operating conditions.

METHODOLOGY

Toroidal micromixer

The toroidal micromixer [7] has become a widely used system for the synthesis of nanoparticles, with applications mainly in the development of drug delivery systems. As shown in Figure 1, it consists of a Y-mixer with additional toroidal mixing elements. The curved geometry of the mixer's channels prompts the formation of Dean flows, which effectively increases the area of contact between the two mixing fluids. As also depicted in Figure 1, the mixer's geometry can be described by the following parameters: channel width and height, number of toroids and their radii, neck angle and length, and Y-mixer entry angle. An additional parameter was considered regarding the smoothness of the geometry's corners ("Corner Length").

Problem formulation

This mixer shape optimization problem aims to maximize the mixing performance for three operating conditions. The TFR value is 10 ml/min for all cases and the FRR values are 1, 2 and 4. The goal is to find the optimal micromixer design for each operating condition and investigate the differences between the obtained geometries. To achieve this, two objectives were considered: minimizing pressure drop, with the goal of minimizing energy consumption but more importantly reducing the risk of device breakage; and minimizing mixing time, which is defined as the characteristic time constant of mixing described as a process of exponential decay of system heterogeneity. Mixing time is used to describe the rate in which the solutions are homogenized, inferring mass-transfer resistance. The mixing time can be estimated from the selectivity analysis of the Villermaux-Dushman competing reactions[5-6].

The evaluations of the two objective functions require the simulation of the system using CFD. This implies the automation of the non-trivial steps of geometry and mesh generation in the CFD simulation workflow. This was done using in-house Python™ code to describe the channel geometries as sets of hexahedral blocks, which were subsequently discretized, using the `blockMesh` utility of OpenFOAM®, to produce the system's mesh.

The complex and expensive nature of the objective functions evaluation calls for the use of efficient optimization algorithms able to locate great performing geometries with minimal number of function evaluations. This is achieved using a Bayesian optimization methodology, as illustrated in Figure 2. In this case, the first 30 system evaluation points were defined using SOBOL sampling. The subsequent 170 points were chosen in a sequential matter by fitting the previously attained data into a Gaussian Process and subsequently maximizing the Expected Hypervolume Improvement function (qEHVI method) [8], totaling 200 function evaluations. The optimization loop was carried out using the Adaptive Experimentation Platform package (Ax-platform) for Python™ [9].

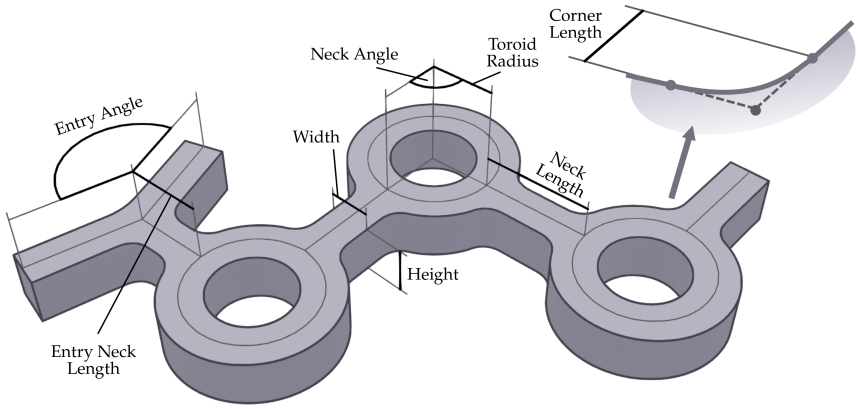

Figure 1. Geometry of the toroidal micromixer and respective parametrization.

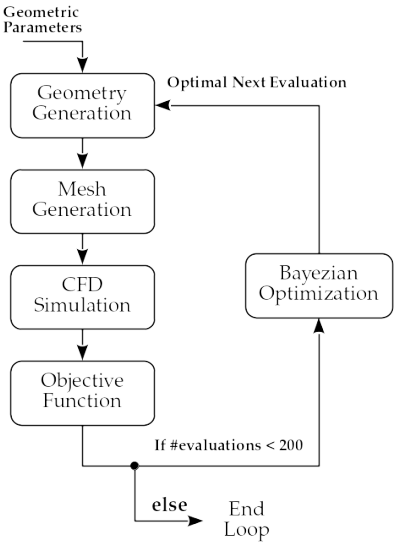

Figure 2. Illustration of the shape optimization loop.

The geometric domain was defined using the aforementioned geometry parametrization of the toroidal mixer and assigning bounds for each parameter, as presented in Table 1. Additional constraints were also implemented in order to avoid the generation of invalid geometries.

Table 1. List of the geometry parameters and additional constraints.

Parameter	Value Range	Units
Entry Angle	[45, 180]	°
Entry Neck Length	[200, 500]	µm
Width	[100, 400]	µm
Height	[0.1, 0.3]	µm
Neck Angle	[90, 270]	°
Neck Length	[200, 700]	µm
Toroid Radius	[100, 600]	µm
# Toroids	[1, 5]	-
Corner Length	[10, 150]	µm
Constraints		
1.5 Width ≤ Toroid Radius		
1.5 Width ≤ Neck Length		
2.2 Corner Length + Width ≤ Neck Length		
2.2 Corner Length + Width ≤ Entry Neck Length		

CFD simulation

In order to evaluate mixer performance, CFD simulations were carried out for each mixer design, considering single-phase, incompressible steady-state flow. Considering the mentioned geometry space, the Reynolds number (Re) range is ≈ [476, 1666], which approaches the upper limit of laminar flow in internal flows. Moreover, the toroidal mixer's geometry is conducive to flow separation and the formation of eddies. A RANS modelling approach was therefore applied using the SST k-ω turbulence model, which is appropriate for lower-Reynolds flows. For boundary conditions, fixed values for velocity and all scalar fields (except pressure) were considered at the inlets. No backflow was allowed at the outlet, and no-slip conditions were considered at the walls. The remaining boundary conditions were modeled as zero gradient conditions. The Villermaux-Dushman reaction is modeled by considering both reactants and reaction products as passive scalars and including the reaction terms in the corresponding transport equations. The reaction kinetics are taken from the literature [6].

The simulations were carried out using OpenFOAM® v2312 and post-processing was done in Python™ using the PyVista package [10].

Villermaux-Dushman Reaction and IEM model

The Villermaux-Dushman competing reaction (Figure 3) consists of a quasi-instantaneous neutralization reaction (R1) and a fast redox reaction (R2) competing for hydrogen ions. The rate of R1 is highly dependent on the mass transfer process and, as such, some hydrogen ions are left to be consumed by the slower reaction (R2). As a result, the selectivity of the Villermaux-Dushman reaction is directly related to mass transfer resistance.

The concept of mixing time (t_m) arises from the Interaction by Exchange with the Mean (IEM) micromixing model, in which mixing time appears as a measure of mass transfer resistance. The model considers two separate volumes of fluid which exchange mass with each other. The mass transfer rate is proportional to the difference in concentration between each volume and the weighted average of both, as written in Equation 1:

$$\begin{cases} \frac{dC_{k,1}}{dt} = \frac{\overline{C_k} - C_{k,1}}{t_m} + R_{k,1} \\ \frac{dC_{k,2}}{dt} = \frac{\overline{C_k} - C_{k,2}}{t_m} + R_{k,2} \\ \overline{C_k} = \alpha C_{k,1} - (1-\alpha) C_{k,2} \end{cases} \quad (1)$$

where $C_{k,1}$, $C_{k,2}$, and $\overline{C_k}$ are the concentrations of species k in volume 1, volume 2, and the weighted average of both, respectively. $R_{k,1}$ and $R_{k,2}$ are the source/sink terms for each species k in volume 1 and 2. Lastly, α and $(1-\alpha)$ correspond to the fractions of volumes 1 and 2 with respect to the total volume.

A calibration curve between mixing time and concentration of the R2 reaction product (I_2) in equilibrium can be obtained by solving the IEM model for a range of mixing time values. Since the relationship between both values is linear, a simple linear regression model can be used. This method is extensively used in literature to experimentally characterize the performance of micromixers [5]. This methodology is implemented here to relate the CFD-simulated I_2 concentration data, at the outlet, with a mixing time value.

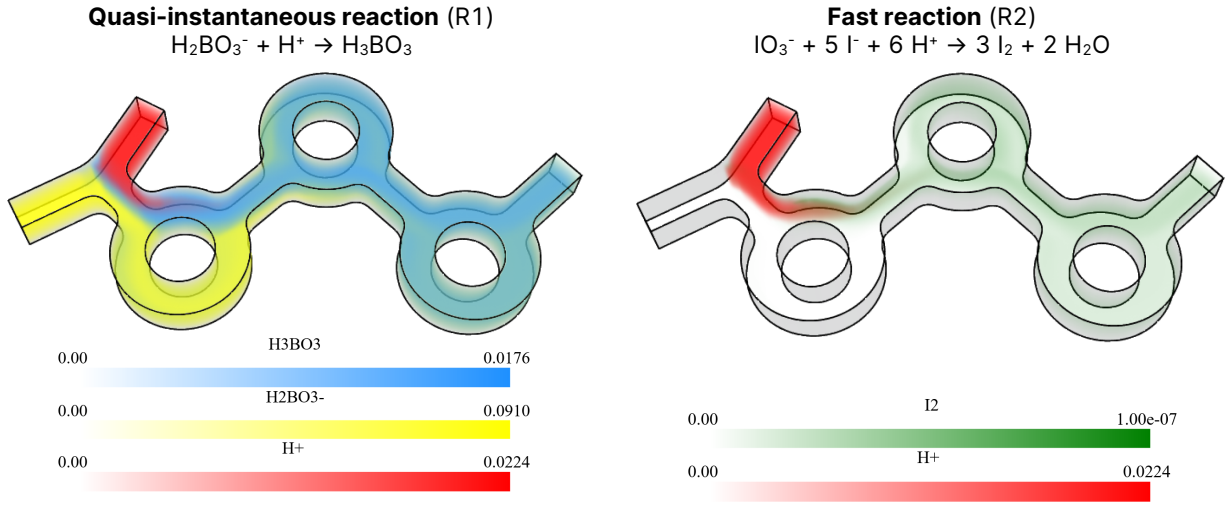

Figure 3. Representation of the CFD simulation of Villermaux-Dushman reaction system. Concentrations of the reactants and product of both reactions are presented in mol.dm^{-3}, using volume rendering of the CFD data of one of the simulations.

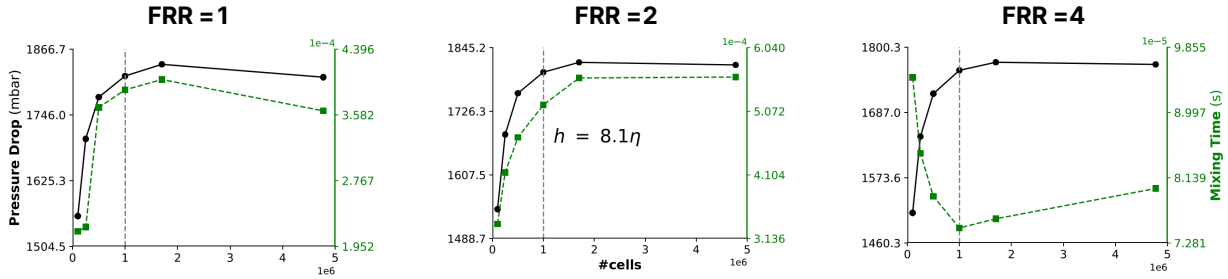

Figure 4. Results of the mesh convergence test. Plot of both objective functions (pressure drop in black and mixing time in green) as a function of the mesh number of cells. The vertical dotted line corresponds to the mesh parameter used in the optimization loop.

Mesh Convergence

The choice of an appropriate mesh is a crucial factor for building faithful CFD models. A grid convergence test was therefore carried out for each operating condition, considering the geometry of the commercially available NanoAssemblr™ Ignite™ cartridge. In Figure 4, both objective functions (ΔP and t_m) are plotted against the number of cells of the respective mesh. Unlike for pressure drop, mixing time convergence was not fully reached. The relation between mixing time and grid size (h) was also not monotonic, likely due to the highly non-linear reaction terms of the Villermaux-Dushman system.

Establishing an appropriate mesh size criteria for all the geometries generated by the optimization algorithm is a non trivial task. It must be robust enough to provide accurate simulations throughout the whole solution space, without producing any type of numerical bias towards any kind of solutions. The criteria should also not be overly conservative to avoid the inefficient use of computational resources in prohibitively expensive meshes. In this case, the Kolmogorov turbulent length scale (η) was used as a reference to determine the appropriate mesh size. From the mesh convergence test, a mesh size of 5.78 µm was chosen as good compromise between model accuracy and computational cost. This corresponded to a grid size 8.1 times larger than the turbulent length scale. This factor was kept constant for the mesh generation throughout the optimization cycles. The turbulent length scale could be estimated prior to mesh generation using Equation 2 [11]:

$$\eta \approx D_h Re^{-3/4} \quad (2)$$

which considers the channel's hydraulic diameter (D_h), calculated with the geometry's height and width values, and the Reynolds number (Re), estimated with the TFR.

RESULTS AND DISCUSSION

The optimization cycle for each value of FRR produces a set of geometry solutions and respective objective function values. These results are illustrated in Figure

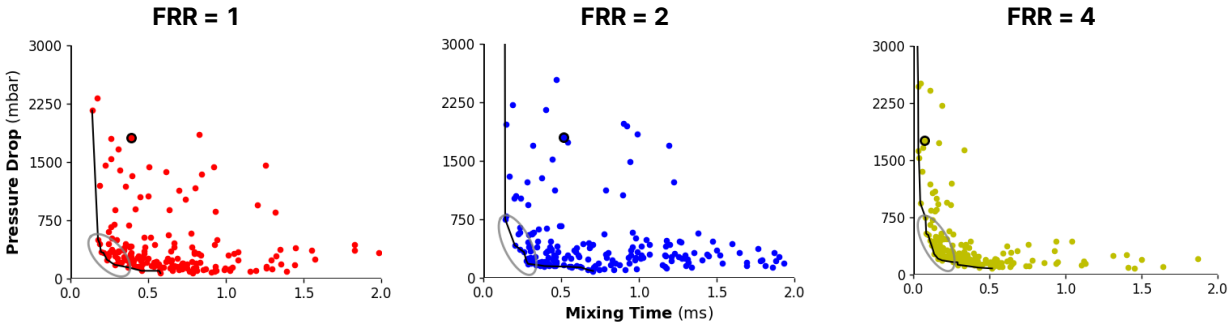

Figure 5. Scatter plot of each solution's objective functions, for each considered FRR. The Pareto front approximation is plotted as black line. The knee fraction of the Pareto front is circled in gray. The point circled in black represents the simulated performance of the reference geometry.

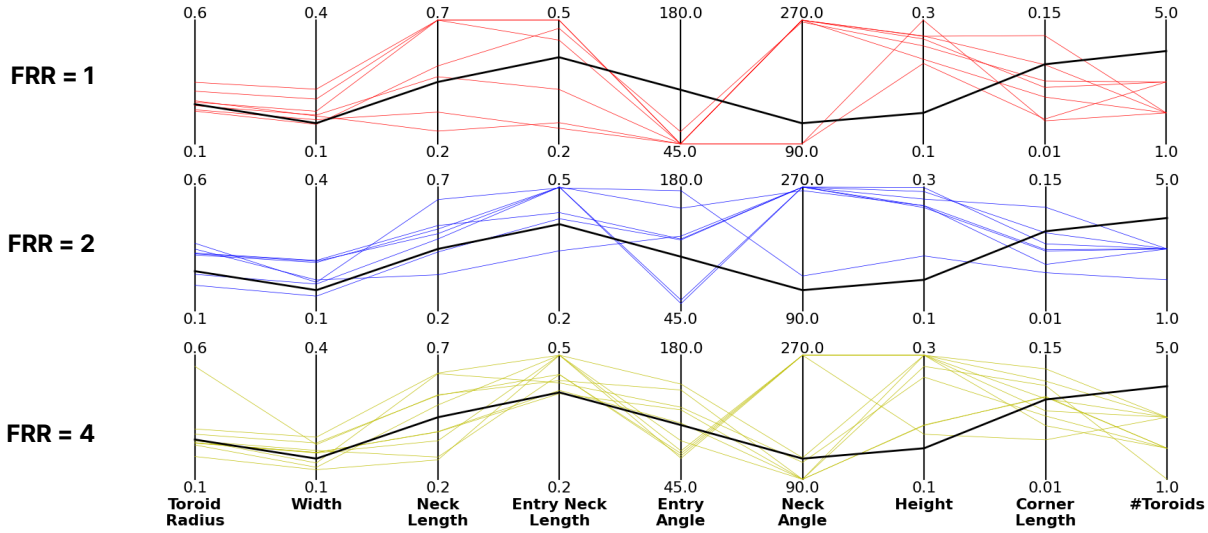

Figure 6. Geometric parameters of the nondominated solutions inside the knee fraction area, for each FRR. The reference geometry parameters are plotted in black.

5, in which the values of the solution's objective functions are compared to the NanoAssemblr™ Ignite™ geometry as a reference. Generally, this reference geometry performed suboptimally when compared to the respective obtained approximation of the Pareto front, in particular for low values of FRR. The main shortcoming being the elevated values of pressure drop.

In Figure 5, the knee fraction of each Pareto front is highlighted within a gray circle. The geometric parameters of the nondominated points of these subsets are presented and compared with the benchmark geometry in Figure 6 for each case study. From these results, it is clear that there is some solution redundancy, as considerably different mixers have similar performance values. This is not surprising, as many engineering problems present the same problem. For this reason, it is difficult to pinpoint how and which geometric parameters are affected by the change in FRR. The clearest exception is the "Entry Angle" parameter which is clearly minimized when FRR = 1 to reduce pressure drop. This is not the case with larger values of FRRs, where the lower flow rate stream is enveloped by the largest one at the inlet junction. This engulfment phenomenon contributes to faster mixing times and is likely enhanced with a wider angle of entry.

Moreover, when comparing the best obtained geometries with the benchmark, the biggest differentiating factor is the increased "Height" of the channels. This has two main effects: first, the cross-sectional area of the channel is increased, reducing pressure drop; second, since the inlets meet laterally, the increase in channel height results in a larger contact area between the flows, promoting mixing. Other significant differences include the reduced number of toroids and the maximization of the "Neck Angle" (90° and 270° produce symmetrical geometries).

Figure 7 illustrates the geometry of good solutions for each FRR value and the reference mixer. Values of the

respective objective function values are also presented. The methodology was able produce improved geometries with a ≈75% reduction of pressure drop in the mixer and a ≈50% reduction in mixing time (except for FRR=4).

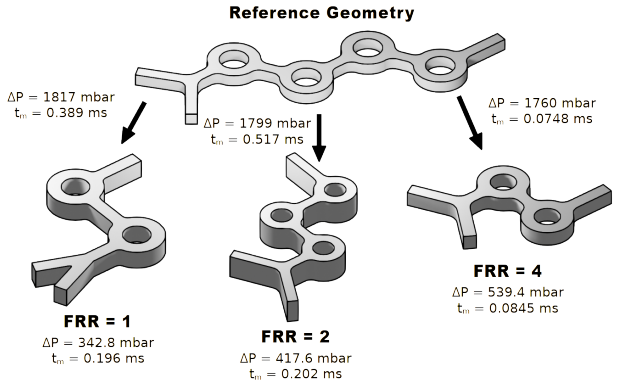

Figure 7. Illustration of the reference geometry and selected solutions for each FRR, and respective objective function values.

CONCLUSION AND PERSPECTIVES

In this work, a shape optimization methodology, using Multi-Objective Bayezian Optimization, was presented and applied to the micromixer design problem. A set of improved geometries were presented and compared to a commercially available reference geometry for three different operating conditions. The most significant geometrical features to mixing performance were identified by analysing the geometrical parameters of the best-found solutions.

The results indicate some discrepancies in the ideal geometry for each operating condition. Thus, future work will consider the formulation of a robust Bayesian optimization framework to optimize the micromixer geometry design for a given range of operating conditions.

ACKNOWLEDGEMENTS

The authors thank financial support from Project “CiNTech - Technological Hub for Innovation, Translation and Industrialization of Complex Injectable Drugs” (reference: 7131), in the scope of PRR - Recovery and Resilience Plan and by the Next Generation EU European Funds, following NOTICE No. 02/C05-i01/2022, Component 5 - Capitalization and Business Innovation - Mobilizing Agendas for Business Innovation.

REFERENCES

1. Alavi SE, Alharthi S, Alavi SF, Alavi SZ, Zahra GE, Raza A, and Shahmabadi HE. Microfluidics for personalized drug delivery. *Drug Discovery Today* 29:103936 (2024).
2. Chen C, Chen C, Li Y, Gu R, and Yan X. Characterization of lipid-based nanomedicines at the single-particle level. *Fundamental Research* 3:488–504 (2023).
3. Pustulka KM, Wohl AR, Lee HS, Michel AR, Han J, Hoye TR, McCormick AV, Panyam J, and Macosko CW. Flash nanoprecipitation: Particle structure and stability. *Molecular Pharmaceutics* 10:4367–4377 (2013).
4. Webb C, Forbes N, Roces CB, Anderluzzi G, Lou G, Abraham S, Ingalls L, Marshall K, Leaver TJ, Watts JA, Aylott JW, Perrie Y. Using microfluidics for scalable manufacturing of nanomedicines from bench to gmp: A case study using protein-loaded liposomes. *International Journal of Pharmaceutics* 582:119266 (2020).
5. Panić S, Loebbecke S, Tuercke T, Antes J, Bošković D. Experimental approaches to a better understanding of mixing performance of microfluidic devices. *Chemical Engineering Journal* 101:409–419 (2004).
6. Commenge JM, Falk L. Villermaux–dushman protocol for experimental characterization of micromixers. *Chemical Engineering and Processing: Process Intensification* 50:979–990 (2011).
7. Wild A, Leaver T, Taylor RJ. Bifurcating mixers and methods of their use and manufacture. US10076730B2 (2016).
8. Daulton S, Balandat M, Bakshy E. Differentiable expected hypervolume improvement for parallel multi-objective bayesian optimization. (2020).
9. Bakshy E, Dworkin L, Karrer B, Kashin K, Letham B, Murthy A, Singh S. AE: A domain-agnostic platform for adaptive experimentation. (2018).
10. Sullivan C, Kaszynski A. Pyvista: 3d plotting and mesh analysis through a streamlined interface for the visualization toolkit (vtk). *Journal of Open Source Software* 4:1450 (2019).
11. Tiselj I, Stalio E, Angeli D, Oder J. Direct numerical simulations for liquid metal applications. In: Thermal Hydraulics Aspects of Liquid Metal Cooled Nuclear Reactors. Ed: Roelofs F. Woodhead Publishing (2019)